

experimental samples in this study, separate spectroscopic experiments strongly suggest that the spin-coating conditions we use to prepare the samples produce films that contain roughly equal amounts of collapsed and non-collapsed conformations. In fact, an equal superposition of the anisotropy distributions H_M of defect-coil and defect-cylinder (V and VI) is in reasonable agreement with the experimental data. Interestingly, the discovery of highly ordered, cylindrical conformations reported here for MEH-PPV may be a critical factor resolving the puzzling properties of MEH-PPV and related polymers. These include the significant local anisotropy of thin films of pure materials²⁴, and evidence that the structure of MEH-PPV in films can be controlled by the conformation in the solution used to spin-coat the films³⁰. The new conformations introduced in the present work, the defect-coil (V) and defect-cylinder (VI), exhibit a key characteristic, namely, structurally identifiable quasi-straight-chain segments. These segments are therefore excellent candidates for the localized quasi-chromophores in conjugated polymers. These conformations probably also describe other stiff-chain conjugated systems, such as polyfluorene and poly(phenyleneethynylene), that can develop the necessary tetrahedral defects. □

Received 10 February; accepted 5 May 2000.

- de Gennes, P.-G. *Scaling Concepts In Polymer Physics* (Cornell Univ. Press, Ithaca, New York, 1979).
- Grosberg, A. Y. & Kuznetsov, D. V. Quantitative theory of the globule-to-coil transition. *Macromolecules* **25**, 1970–2003 (1992).
- Friend, R. H. *et al.* Electroluminescence in conjugated polymers. *Nature* **397**, 121–128 (1999).
- Hide, F., Diazgarcia, M. A., Schwartz, B. J. & Heeger, A. J. New developments in the photonic applications of conjugated polymers. *Acc. Chem. Res.* **30**, 430–436 (1997).
- Yang, C. Y., Hide, F., Diazgarcia, M. A., Heeger, A. J. & Cao, Y. Microstructure of thin films of photoluminescent semiconducting polymers. *Polymer* **39**, 2299–2304 (1998).
- Bloomfield, V. A. Condensation of DNA by multivalent cations: Consideration on mechanism. *Biopolymers* **31**, 1471–1481 (1991).
- Grosberg, A. Y. Certain possible conformational states of a uniform elastic polymer chain. *Biophysics* **24**, 30–36 (1979).
- Ivanov, V. A., Paul, W. & Binder, K. Finite chain length effects on the coil-globule transition of stiff-chain macromolecules—a Monte Carlo simulation. *J. Chem. Phys.* **109**, 5659–5669 (1998).
- Noguchi, H. & Yoshikawa, K. Morphological variation in a collapsed single homopolymer chain. *J. Chem. Phys.* **109**, 5070–5077 (1998).
- Zhou, Y. Q., Karplus, M., Wichert, J. M. & Hall, C. K. Equilibrium thermodynamics of homopolymers and clusters - molecular dynamics and Monte Carlo simulations of systems with square-well interactions. *J. Chem. Phys.* **107**, 10691–10708 (1997).
- Kuznetsov, Y. A. & Timoshenko, E. G. On the conformational structure of a stiff homopolymer. *J. Chem. Phys.* **111**, 3744–3752 (1999).
- Xie, X. S. & Trautman, J. K. Optical studies of single molecules at room temperature. *Annu. Rev. Phys. Chem.* **49**, 441–480 (1998).
- Basche, T., Moerner, W. E., Orrit, M. & Wild, U. P. (eds) *Single Molecule Optical Detection, Imaging, and Spectroscopy* (Verlag Chemie, Munich, 1996).
- Ha, T., Laurence, T. A., Chempla, D. S. & Weiss, S. Polarization spectroscopy of single fluorescent molecules. *J. Phys. Chem. B* **103**, 6839–6850 (1999).
- Vandenbout, D. A. *et al.* Discrete intensity jumps and intramolecular electronic energy transfer in the spectroscopy of single conjugated polymer molecules. *Science* **277**, 1074–1077 (1997).
- Hu, D., Yu, J. & Barbara, P. F. Single-molecule spectroscopy of the conjugated polymer MEH-PPV. *J. Am. Chem. Soc.* **121**, 6936–6937 (1999).
- Yaliraki, S. N. & Silbey, R. J. Conformational disorder of conjugated polymers—implications for optical properties. *J. Chem. Phys.* **104**, 1245–1253 (1996).
- Gettinger, C. L., Heeger, A. J., Drake, J. M. & Pine, D. J. A photoluminescence study of poly(phenylene vinylene) derivatives—the effect of intrinsic persistence length. *J. Chem. Phys.* **101**, 1673–1678 (1994).
- Padmanaban, G. & Ramakrishnan, S. Conjugation length control in soluble poly[2-methoxy-5-(2'-ethylhexyl)oxy-1,4-phenylenevinylene] (MEHPPV): synthesis, optical properties, and energy migration. *J. Am. Chem. Soc.* **122**, 2244–2251 (2000).
- Mukamel, S., Tretiak, S., Wagersreiter, T. & Chernyak, V. Electronic coherence and collective optical excitations of conjugated molecules. *Science* **277**, 781–787 (1997).
- Woo, H. S. *et al.* Optical spectra and excitations in phenylene vinylene oligomers. *Synth. Met.* **59**, 13–28 (1993).
- Hagler, T. W., Pakbaz, K. & Heeger, A. J. Polarized-electroabsorption spectroscopy of a soluble derivative of poly(p-phenylenevinylene) oriented by gel processing in polyethylene—polarization anisotropy, the off-axis dipole moment, and excited-state delocalization. *Phys. Rev. B* **49**, 10968–10975 (1994).
- Bassler, H. & Schweitzer, B. Site-selective fluorescence spectroscopy of conjugated polymer and oligomers. *Acc. Chem. Res.* **32**, 173–182 (1999).
- Blatchford, J. W. *et al.* Spatially and temporally resolved emission from aggregates in conjugated polymers. *Phys. Rev. B* **54**, R3683–R3686 (1996).
- Thulstrup, E. W. & Michl, J. *Elementary Polarization Spectroscopy* (VCH, New York, 1989).
- Carmesin, I. & Kremer, K. The bond fluctuation method: a new effective algorithm for the dynamics of polymers in all spatial dimensions. *Macromolecules* **21**, 2819–2823 (1988).
- Helfand, E. Theory of the kinetics of conformational transitions in polymer. *J. Chem. Phys.* **54**, 4651–4661 (1971).

- Orion, I., Buisson, J. P. & Lefrant, S. Spectroscopic studies of polaronic and bipolaronic species in n-doped poly(paraphenylenevinylene). *Phys. Rev. B* **57**, 7050–7065 (1998).
- Lodge, T. P. & Fredrickson, G. H. Optical anisotropy of tethered chains. *Macromolecules* **25**, 5643–5650 (1992).
- Nguyen, T. Q., Doan, V. & Schwartz, B. J. Conjugated polymer aggregates in solution: Control of interchain interactions. *J. Chem. Phys.* **110**, 4068–4078 (1999).

Acknowledgements

This work was supported by grants from the National Science Foundation (P.F.B.), the Robert A. Welch Foundation (P.J.R. & P.F.B.), and the Texas Advanced Research Program (P.J.R.). Further support was provided by the Institute for Theoretical Chemistry and by the Laboratory for Spectroscopic Imaging, University of Texas. We also thank A. Yethiraj for discussions.

Correspondence and requests for materials should be addressed to P.F.B. (e-mail: p.barbara@mail.utexas.edu).

Dynamic self-assembly of magnetized, millimetre-sized objects rotating at a liquid–air interface

Bartosz A. Grzybowski*, Howard A. Stone† & George M. Whitesides*

*Harvard University, Department of Chemistry and Chemical Biology, 12 Oxford Street, Cambridge, Massachusetts 02138, USA

†Harvard University, Division of Engineering and Applied Sciences, Pierce Hall, Cambridge, Massachusetts 02138, USA

Spontaneous pattern formation by self-assembly is of long-standing^{1–3} and continuing interest^{4,5} not only for its aesthetic appeal^{6,7}, but also for its fundamental^{8–18} and technological relevance¹⁹. So far, the study of self-organization processes has mainly focused on static structures, but dynamic systems^{20–22}—those that develop order only when dissipating energy—are of particular interest for studying complex behaviour^{23,24}. Here we describe the formation of dynamic patterns of millimetre-sized magnetic disks at a liquid–air interface, subject to a magnetic field produced by a rotating permanent magnet. The disks spin around their axes with angular frequency equal to that of the magnet, and are attracted towards its axis of rotation while repelling each other. This repulsive hydrodynamic interaction is due to fluid motion associated with spinning; the interplay between attractive and repulsive interactions leads to the formation of patterns exhibiting various types of ordering, some of which are entirely new. This versatile system should lead to a better understanding of dynamic self-assembly, while providing a test-bed for stability theories of interacting point vortices^{25–28} and vortex patches²⁹.

We fabricated circular disks by filling hollow polyethylene tubing (~1 mm inside diameter, ~2 mm outside diameter) with poly(dimethylsiloxane) (PDMS) doped with magnetite (~5–30 wt%), and cutting the resulting composite into slices ~400 μm thick. A permanent bar magnet of approximate dimensions ($L \times W \times D$, in cm) $5.6 \times 4 \times 1$ was placed at a distance h (about 2–4 cm) below the interface, and rotated with angular velocity ω (Fig. 1a). The magnet was magnetized along its longest dimension, and had magnetization $M \approx 1,000 \text{ G cm}^{-3}$. When the magnet was stationary, the disks were attracted towards its poles, where they formed orderless aggregates. When the magnet rotated, the disks were drawn towards its axis of rotation. In addition, the magnetic moments of the disks interacted with the rotating magnetic field, and the disks spun around their centres. The fluid motion associated with spinning resulted in a repulsive hydrodynamic

interaction between the disks.

The competition between axisymmetric magnetic attraction and hydrodynamic repulsion of the disks led to the formation of ordered aggregates (Fig. 2). We denote the number of disks in an aggregate by n . One disk ($n = 1$) experiences only the attractive magnetic force, and in its stable position, its centre coincides with the axis of rotation of the magnet (we will use “the centre” to mean this axis of rotation). For $n = 2$, the disks repel each other, and are equidistant from the centre, around which they slowly precess (angular velocity $\Omega \approx 2$ r.p.m.). For $n = 3-5$, the disks organize into polygons (a triangle for $n = 3$, a square for $n = 4$, and a pentagon for $n = 5$) precessing around the centre. For $n = 6$, one disk goes to the centre, while the remaining five form a pentagon around it. For $n > 6$, multishell structures appear. The shells precess with the same angular velocity Ω . Most of the aggregates have one, well defined stable structure, but in three cases we observed polymorphs, where multiple steady states are possible. For 10 and 12 disks, the patterns spontaneously interconvert between the polymorphs. In the 19-membered aggregate, the hexagonal structure (shown on

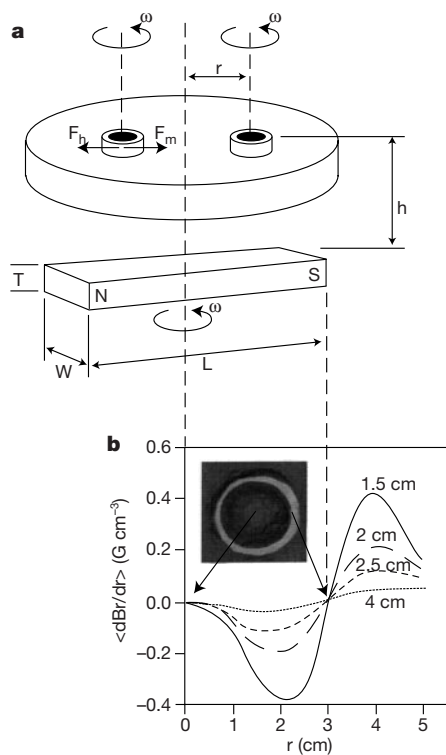


Figure 1 Experimental set-up and magnetic force profiles. **a**, A scheme of the experimental set-up. A bar magnet rotates at angular velocity ω below a dish filled with liquid (typically ethylene glycol/water or glycerine/water solutions). Magnetically doped disks are placed on the liquid–air interface, and are fully immersed in the liquid except for their top surface. The disks spin at angular velocity ω around their axes. A magnetic force F_m attracts the disks towards the centre of the dish, and a hydrodynamic force F_h pushes them apart from each other. The curves in **b** give the time average (over one revolution of the magnet) of the radial derivative of the magnetic induction $\partial B_r/\partial r$ as a function of r . This derivative is proportional to the radially directed magnetic force $F_m(r)$ acting on a ferromagnetic point object located at r . Each curve corresponds to a different separation h between the upper face of the magnet and the liquid–air interface. The force is ‘attractive’ (directed towards the centre) for $r < \sim 3$ cm (roughly equal to $L/2$, half of the length L of the magnet), and ‘repulsive’ otherwise. The patterns are stable only within the attractive region. Inset, an optical micrograph showing the results of an experiment with iron filings suspended in a viscous oil, and subjected to a rotating magnetic field such as that used in the calculations: the annular band where F_m changes sign (near $r \approx L/2$) is depleted of filings.

the left in Fig. 2) appears only above a threshold rotational speed $\omega \approx 800$ r.p.m., while the less symmetric structure (shown on the right) exists below this value (although the hexagonal structure can be sustained in a metastable equilibrium at $\omega < 800$ r.p.m. by slowly decreasing ω from above the threshold). The aggregate formed by 19 1.27-mm disks is the largest stable structure observed with the magnet used in our experiments. The reason for this limitation is

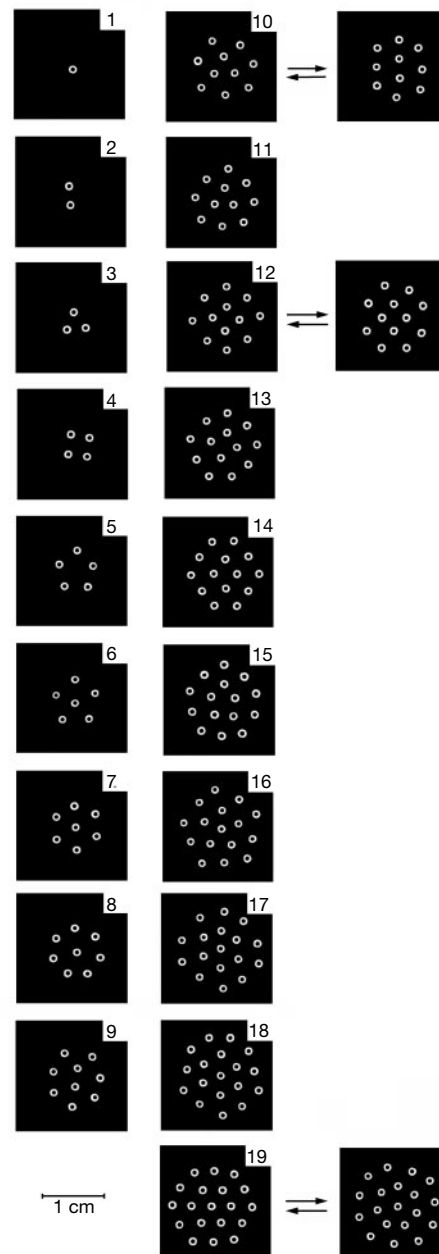


Figure 2 Dynamic patterns formed by various numbers (n) of disks rotating at the ethylene glycol/water–air interface. This interface is 27 mm above the plane of the external magnet. The disks are composed of a section of polyethylene tube (white) of outer diameter 1.27 mm, filled with poly(dimethylsiloxane), PDMS, doped with 25 wt% of magnetite (black centre). All disks spin around their centres at $\omega = 700$ r.p.m., and the entire aggregate slowly ($\Omega < 2$ r.p.m.) precesses around its centre. For $n < 5$, the aggregates do not have a ‘nucleus’—all disks are precessing on the rim of a circle. For $n > 5$, nucleated structures appear. For $n = 10$ and $n = 12$, the patterns are bistable in the sense that the two observed patterns interconvert irregularly with time. For $n = 19$, the hexagonal pattern (left) appears only above $\omega \approx 800$ r.p.m., but can be ‘annealed’ down to 700 r.p.m. by slowly decreasing the spinning rate. Without annealing, a less symmetric pattern exists at $\omega = 700$ r.p.m.

that, as the aggregate gets bigger, the outermost disks experience a less-homogenous and weaker magnetic field than those closer to the centre. Under such conditions, they often fall out of resonance with the external rotating field and stop spinning.

The spacing between the nearest neighbours in an aggregate of size n is approximately independent of n , but increases with increasing ω . The faster a disk spins, the larger the hydrodynamic repulsion it exerts on other disks. Thus, for a given strength of the magnetic field, the separation between the disks increases with ω . Figure 3a shows two aggregates of 860- μm -diameter disks: in the picture on the left ($\omega \approx 800$ r.p.m.), the lattice spacing is smaller than in the picture on the right, where the disks are rotating at $\omega \approx 1,100$ r.p.m. (notice the outer disordered rim, where the disks are off-resonance with the magnetic field). The lattice spacing can be increased only to about seven disk diameters: above this separation, disks start moving independently from each other, and the ordering disappears (Fig. 3b).

The largest aggregates obtained in our experiments were hexagonal structures, shown in Fig. 3c. Here the disks were 570 μm in diameter; because of their small size, many disks could be packed into the region of homogeneous magnetic field. The magnetite content in these disks was low (~ 5 wt%), to minimize their tilting or tumbling. The structures were stable only when the packing in the aggregate was hexagonal, and the structure had a six-fold symmetry.

To understand better the nature and the capabilities of self-

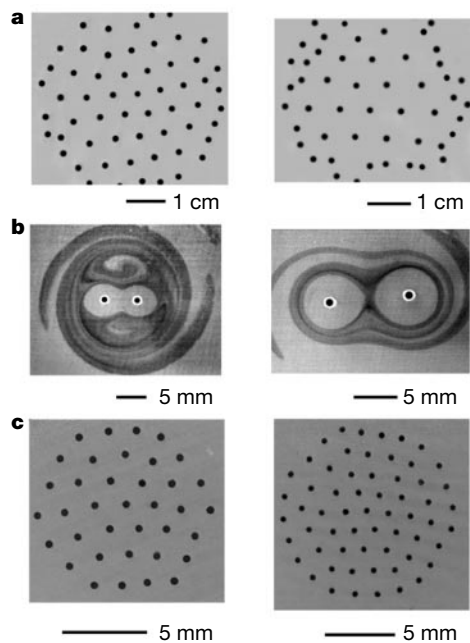


Figure 3 Illustrations of various effects controlling the dimensions and the stability of patterns. In **a**, the lattices were formed by 0.86-mm disks; the lattice spacing increased with the rotational speed (800 r.p.m. in the picture on the left, 1,100 r.p.m. in the picture on the right). The pictures in **b** illustrate the effect of ω on the stability of aggregates. Two 1.27-mm disks were spinning on the ethylene glycol–water interface. The streamlines were visualized by placing drops of rhodamine/water solution onto the interface. In the picture on the left, the disks were rotating at $\omega = 700$ r.p.m. No dye entered a high-pressure ‘8-shaped’ region connecting the rotating disks, and the separation between the disks did not change with time. When ω was increased to 1,100 r.p.m., the high-pressure regions produced by the disks became disjoint, as indicated by the crossing of the streamlines in the midpoint between the disks (right). Disks moved independently of each other, and the separation between them varied with time. Optical micrographs in **c** show hexagonally ordered aggregates formed by 570- μm PDMS disks doped with 5% magnetite, and rotating at $\omega = 1,100$ r.p.m. on a liquid–air interface 2.5 cm above the top face of the magnet. In this experiment, the liquid was a solution of 75% ethylene glycol:25% water.

assembly in our system, we investigated the forces involved in the process both theoretically and experimentally. We calculated the magnetic force acting on the disks using a standard current-sheet method (see Supplementary Information); profiles of the magnetic force are shown in Fig. 1b. The hydrodynamic repulsive forces arise from the combination of the spinning of a disk and its translation through the liquid. Consider the simplest aggregate composed of two disks. Each disk produces a rotational flow of liquid around it, and also experiences a flow produced by the other disk. Thus, each disk can be represented as rotating around its axis, while simultaneously translating through the flow with a gradient of shear produced by the other disk. For the typical rotation speeds (ω), disk radii (a), densities (ρ) and fluid shear viscosities (μ) of our experiments, the Reynolds number on the scale of the particle is $Re = (\rho\omega a^2/\mu) < O(1)$, although it is not very much smaller (here, we use the symbol $O(\epsilon)$ to mean, as usual, ‘order-of- magnitude’ of ϵ). We note that an explanation based on the Bernoulli principle appears inappropriate, because the Reynolds number is small.

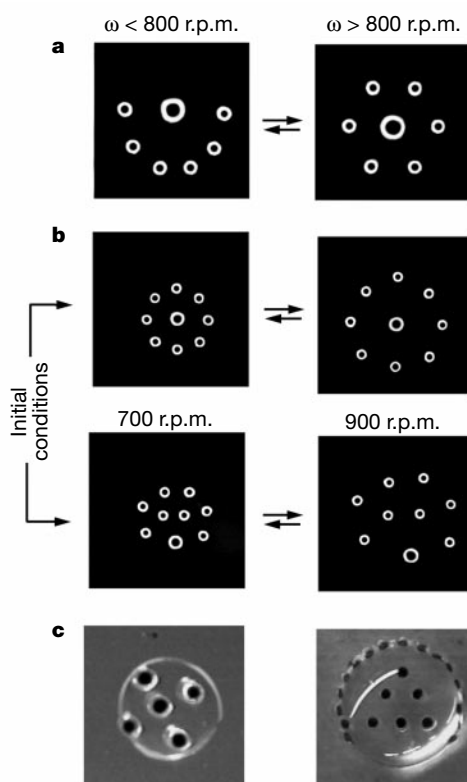


Figure 4 Various phenomena observed in systems of magnetized rotating disks. In **a** the two structures interconvert depending on the rotational speed ω of the external magnet. For $\omega < \sim 800$ r.p.m., both the small disks (1.27 mm in diameter), and the large disk (2.42 mm in diameter), rotate at ω ; the small disks organize in a semicircle slowly precessing around the large disk. When ω is increased, the large disk falls off resonance from the external magnetic field, and starts rotating at $\omega' < \omega$. As a result, the hydrodynamic repulsion it exerts on its smaller neighbours decreases; the structure of the aggregate changes, and resembles the one formed by seven equally sized disks (Fig. 2). In **b** the difference in size between the large disk (diameter 1.7 mm) and the small disks (1.27 mm) is not large enough to ensure that the large disk will always organize smaller disks around it; the type of aggregate formed depends on initial conditions. Once either of the two types is formed, its size can be modified by adjusting ω , but the two morphologies cannot be interconverted. The optical micrographs in **c** show aggregates assembled on curved surfaces; we did not observe such structures in our experiments on planar interfaces. The picture on the left shows a nucleated five-membered aggregate of 1.27-mm disks rotating on the top surface of a droplet of perfluorodecalin (PFD) covered with water. The picture on the right shows a pattern formed on the bottom of a water droplet floating on a PFD–air interface.

We thus expect the explanation for the repulsive hydrodynamic interaction to lie in the realm of viscosity-dominated flows, where small inertial effects are probably significant. There are only a few analytical results available for a force-free particle in a wall-bounded shear flow³⁰: such a particle experiences a lift force transverse to the streamlines $O(\mu u_C a Re_G)$, where u_C is the typical velocity on the scale of the particle, and $Re_G = \rho G a^2 / \mu$ is the Reynolds number based on the local shear rate G . For our system, the particle experiences a torque, which generates a local velocity $u_C = \omega a$, and the background shear rate is $G = O(\omega a^3 / d^3)$, where d is the distance between the centres of the disks. Therefore, the repulsive hydrodynamic force F_h between the disks is predicted to be $F_h = O(\mu(\omega a) a Re_G) = O(\rho \omega^2 a^7 / d^3)$. In the stable configuration, this hydrodynamic repulsion balances the magnetic force attracting the disks towards the axis of rotation of the external magnet. Although a detailed calculation remains to be done, we verified experimentally that qualitative trends predicted by this analysis appear to be correct (see Supplementary Information).

Our qualitative theory explains the nature of the pairwise forces acting in the system, but it is clearly insufficient to account for the emergence of the patterns that we observe, especially in more complicated systems. The structure of the aggregates of disks of different sizes can be controlled by adjusting the rotational speed to decouple larger disks from the field selectively (Fig. 4a). Aggregates that have structures dependent on the initial distribution of the disks can also be prepared (Fig. 4b). The self-assembly can take place on both planar and curved surfaces (Fig. 4c). It seems likely that changing the shape of the spinners, and engineering the profile of the magnetic field, would lead to even more complex behaviour.

We believe that this system could be a useful experimental tool in assisting theoretical research on multivortex flows. Also, if the size of the disks could be reduced to several micrometres, the type of self-assembly that we describe here might have practical applications in optics; for example, in tunable diffraction gratings or in photonic bandgap materials. If it was found to be possible to 'solidify' large, dynamic structures, new materials or materials precursors (such as membranes and molecular sieves) might be obtained. □

Received 16 December 1999; accepted 10 April 2000.

- Mayer, A. M. Floating magnets. *Nature* **18**, 258–260 (1878).
- Derr, L. A photographic study of Mayer's floating magnets. *Proc. Am. Acad. Arts Sci.* **44**, 525–528 (1909).
- Monckman, J. On the arrangement of electrified cylinders when attracted by an electrified sphere. *Proc. Camb. Phil. Soc.* **6**, 179–181 (1888).
- Schecter, D. A., Dubin, D. H. E., Fine, K. S. & Driscoll, C. F. Vortex crystals from 2D Euler flow: experiment and simulation. *Phys. Fluids* **11**, 905–914 (1999).
- Bubeck, R., Bechinger C., Nesor, S. & Leiderer, P. Melting and reentrant freezing of two-dimensional colloidal crystals in confined geometry. *Phys. Rev. Lett.* **82**, 3364–3367 (1999).
- Ghyka, M. *The Geometry of Art and Life* (Dover, New York, 1977).
- Ball, P. *The Self-Made Tapestry: Pattern Formation in Nature* (Oxford Univ. Press, New York, 1999).
- Whitesell, J. K. *Organised Molecular Assemblies in the Solid State* (Wiley, New York, 1999).
- Philp, D. & Stoddart, J. F. Self-assembly in natural and unnatural systems. *Angew. Chem. Int. Edn Engl.* **35**, 1155–1196 (1996).
- Lounasmaa, O. V. & Thuneberg, E. Vortices in rotating superfluid ³He. *Proc. Natl Acad. Sci. USA* **96**, 7760–7767 (1999).
- Bowden, N., Brittain, S., Evans, A. G., Hutchinson, J. W. & Whitesides, G. M. Spontaneous formation of ordered structures in thin films of metals supported on an elastomeric polymer. *Nature* **393**, 146–149 (1998).
- Bowden, N., Choi, I. S., Grzybowski, B. A. & Whitesides, G. M. Mesoscale self-assembly of hexagonal plates using lateral capillary forces: synthesis using the "capillary bond". *J. Am. Chem. Soc.* **121**, 5373–5391 (1999).
- Shinbrot, T. Competition between randomizing impacts and inelastic collisions in granular pattern formation. *Nature* **389**, 574–576 (1997).
- Burns, M. M., Fournier, J. M. & Golovchenko, J. A. Optical matter—crystallization and binding in intense optical fields. *Science* **249**, 749–754 (1990).
- Murray, C. A. & Grier, D. G. Colloidal crystals—solid particles suspended in fluid form ordered arrays with unusual and useful physical properties. *Am. Sci.* **83**, 238–245 (1995).
- Thompson, D'A. *On Growth and Form* (Dover, New York, 1992).
- Shapiro, J. A. Thinking about bacterial populations as multicellular organisms. *Annu. Rev. Microbiol.* **52**, 81–104 (1998).
- Berg, H. & Budrene, E. O. Dynamics of formation of symmetrical patterns by chemotactic bacteria. *Nature* **376**, 49–53 (1995).
- GomezLopez, M., Preece, J. A. & Stoddart, J. F. The art and science of self-assembling molecular

machines. *Nanotechnology* **7**, 183–192 (1996).

- Koschmieder, A. *Benard Cells and Taylor Vortices* (Cambridge Univ. Press, New York, 1993).
- Jakubith, S., Rotermund, H. H., Engel, W., von Oertzen, A. & Ertl, G. Spatiotemporal concentration patterns in a surface reaction: propagating and standing waves, rotating spirals, and turbulence. *Phys. Rev. Lett.* **65**, 3013–3016 (1990).
- Engelborghs, Y. Microtubules—dissipative structures formed by self-assembly. *Biosens. Bioelectron.* **9**, 685–689 (1994).
- Lindgren, K., Moore, C. & Nordahl, M. Complexity of two-dimensional patterns. *J. Stat. Phys.* **91**, 909–951 (1998).
- Singh, R., Maru, V. M. & Moharir, P. S. Complex chaotic systems and emergent phenomena. *J. Nonlinear Sci.* **8**, 235–259 (1998).
- Havelock, T. H. The stability of motion of rectilinear vortices in ring formation. *Phil. Mag.* **11**, 617–633 (1931).
- Morton, W. B. Vortex polygons. *Proc. R. Irish Acad. A* **42**, 21–29 (1935).
- Aref, H. & Vainchtein, D. L. Point vortices exhibit asymmetric equilibria. *Nature* **392**, 769–770 (1998).
- Thomson, J. J. *A Treatise on the Motion of Vortex Rings* (Macmillan, London, 1883).
- Dritschel, D. G. The stability and energetics of corotating uniform vortices. *J. Fluid Mech.* **157**, 95–134 (1985).
- Schonberg, J. A. & Hinch, E. J. Inertial migration of a sphere in Poiseuille flow. *J. Fluid Mech.* **203**, 517–524 (1989).

Supplementary Information is available on Nature's World-Wide Web site (<http://www.nature.com>) or as paper copy from the London editorial office of Nature.

Acknowledgements

This work was supported by DARPA and NSF.

Correspondence and requests for materials should be addressed to G.M.W. (e-mail: gwhitesides@gmwgroup.harvard.edu).

Structural basis for the fracture toughness of the shell of the conch *Strombus gigas*

S. Kamat*, X. Su*, R. Ballarini† & A. H. Heuer*

* Department of Materials Science and Engineering, † Department of Civil Engineering, Case Western Reserve University, Cleveland, Ohio 44106-7204, USA

Natural composite materials are renowned for their mechanical strength and toughness: despite being highly mineralized, with the organic component constituting not more than a few per cent of the composite material, the fracture toughness exceeds that of single crystals of the pure mineral by two to three orders of magnitude¹. The judicious placement of the organic matrix, relative to the mineral phase, and the hierarchical structural architecture extending over several distinct length scales both play crucial roles in the mechanical response of natural composites to external loads^{2–4}. Here we use transmission electron microscopy studies and beam bending experiments to show that the resistance of the shell of the conch *Strombus gigas* to catastrophic fracture can be understood quantitatively by invoking two energy-dissipating mechanisms: multiple microcracking in the outer layers at low mechanical loads, and crack bridging in the shell's tougher middle layers at higher loads. Both mechanisms are intimately associated with the so-called crossed lamellar microarchitecture of the shell, which provides for 'channel' cracking in the outer layers and uncracked structural features that bridge crack surfaces, thereby significantly increasing the work of fracture, and hence the toughness, of the material. Despite a high mineral content of about 99% (by volume) of aragonite, the shell of *Strombus gigas* can thus be considered a 'ceramic plywood', and can guide the biomimetic design of tough, lightweight structures.

The crossed lamellar shell of *Strombus gigas*, the giant pink Queen conch native to Caribbean habitats, contains structure at five